PROCEEDINGS OF SCIENCE

Oscillating Autocorrelation and the HMC Algorithm

Falk Zimmermann*

Helmholtz Institute for Radiation and Nuclear Physics, University of Bonn
Nußallee 14-16, 53115 Bonn, Germany

E-mail: fzimmermann@hiskp.uni-bonn.de

The study of autocorrelation times of various meson operators and the topological charge revealed the presence of hidden harmonic oscillations of the autocorrelations (for the HMC). These modes can be extracted by smoothing the observables with respect to the Monte Carlo time. While this smoothing procedure removes the largest share of the operator's signal, it can not be excluded that physically relevant contributions remain coupled to the oscillations. Furthermore, common statistical error analysis relies on binning and, thus, is not suited to remove non-decaying forms of autocorrelation. I present a new error analysis framework that is based on defining an effective number of independent measurements via the ratio of the entropy of the correlated data distribution excluding autocorrelation and the entropy of the distribution including autocorrelation. This framework is used to show that the autocorrelation oscillations are significant. I argue that the oscillations could be understood in terms of a 5D theory involving the Molecular dynamics momenta and are manifestations of the theoretical modes used by the Fourier acceleration approach. FA might control the modes and suppress their impact on the simulated physics.

The 39th International Symposium on Lattice Field Theory (Lattice2022),
8-13 August, 2022
Bonn, Germany

*Speaker

PoS(LATTICE2022)045

1. Introduction: autocorrelation field of correlator fluctuations

For any two correlation functions $c_a(t,\tau)$, $c_b(t,\tau)$, that are given at lattice configurations enumerated by τ, one can define their mutual, ensemble-wide correlation via:

$$\mathrm{corr}_{\mathrm{fc}}[c_a, c_b] \;=\; \frac{\sum_{\tau=1}^{N}\sum_{t=1}^{T}(c_a(t,\tau)-\langle c_a\rangle_\tau(t))\cdot(c_b(t,\tau)-\langle c_b\rangle_\tau(t))}{TN\sigma_a\sigma_b} \tag{1}$$

where T is the time-like extend of the lattice and N the number of configurations. In order to compute meaningful $\mathrm{corr}_{\mathrm{fc}}$ for different physical correlation functions $c_{a/b}(t)$, the mean value $\langle c_{a/b}\rangle(t)$ must be subtracted for each t, respectively: The remaining fields $c(t,\tau)-\langle c\rangle_\tau(t)$ consist of (quantum) noise, fluctuations accounting for variations of the underlying physical context (topological charge...), and possible lattice artefacts. The second and third kinds of fluctuations may contribute to both fields $\bar{c}_{a/b}$ and will then result in a non-zero $\mathrm{corr}_{\mathrm{fc}} \in [-1,1]$. In this proceeding, we focus on the artefacts that produce harmonic oscillations of the autocorrelation (AC) field:

$$\Gamma[c_a, c_b](t,\Delta\tau) \;=\; \frac{\sum_{\tau=1}^{N-\Delta\tau}(c_a(t,\tau)-\langle c_a\rangle_\tau(t))\cdot(c_b(t,\tau+\Delta\tau)-\langle c_b\rangle_\tau(t))}{(N-\Delta\tau)\sigma_\tau[c_a](t)\sigma_\tau[c_b](t)} \tag{2}$$

1.1 Smoothed correlation functions

While the Hybrid Monte-Carlo algorithm traverses the QCD configuration space, certain excitations prove to be more resilient to that updating procedure than others. Smoothing correlators with respect to the iteration number τ removes much noise and uncovers the resilient features. For example it has been used to study the topological charge in the past.

$$\bar{c}_{\mathrm{IR}_\lambda}(t,\tau) \;\equiv\; \sum_{\tau'=1}^{N}\bar{c}(t,\tau')\frac{1}{\sqrt{2\pi\lambda^2}}e^{-\frac{(\tau-\tau')^2}{2\lambda^2}} \tag{3}$$

This smoothed function might be called the IR part of $\bar{c} = \bar{\bar{c}} - \langle\bar{\bar{c}}\rangle_\tau$ concerning the chosen scale λ. In the following, we need to deal only with $\bar{c}_{\mathrm{IR}_\lambda}(t,\tau)$ made from two-point functions $\bar{\bar{c}}_{\hat{o}_a\hat{o}_{b=a}}$, having the same lattice operator $\hat{o}_a$ at source and sink. Hence, in order to simplify the notation, we will just write $\bar{c}_{\hat{o}}$ for IR-smoothed fluctuation corresponding to $\hat{o}$.

1.2 Normalisation with respect to the physical time

Quark-disconnected fields $\bar{c}_{\mathrm{disc}}(\tau,t)$ and those made from topological correlation functions usually do not require a t-dependent normalisation - the standard deviation does not alter noticeably with respect to t. The quark-connected fluctuation fields $\bar{c}_{\mathrm{conn}}$ possess a standard deviation $\sigma_\tau[\bar{c}_{\mathrm{conn}}](t) \propto e^{-mt}$ which is most easily normalised by

$$c(t,\tau) \;\equiv\; \frac{\bar{c}(t,\tau)-\langle\bar{c}\rangle_\tau(t)}{\sigma_\tau[\bar{c}](t)}\,. \tag{4}$$

As an immediate consequence, we end up with a noise field with a variance homogeneous in t and τ. Note that for $\lambda = 0$, c still contains almost all information. Now it is possible to define the last

version of the fluctuation field, where we remove the time average on a per-configuration basis[1]:

$$\tilde{c}(t,\tau) \equiv c(t,\tau) - \langle c \rangle_{t\in[t_0,T]}(\tau) \tag{5}$$

1.3 Data sets and considered latticed operators

The analysis has been carried out by focusing on three ensemblesof the ETM Collaboration [1]:

B55.32 (L=32, T=64, N≈4900), **A40.24** (L=24, T=32, N≈1100), **A60.24:** (L=24, T=32, N≈1250)

Because of the constrained length of this work, we will only show results for the ensemble with the highest statistic (B55). The fluctuation fields have been created from two-point functions with the same lattice operator at source and sink. We group them into tuples:

- Neutral operators used to build light quark-connected correlators (twisted mass basis):

$$\hat{O}_l \equiv \left(\text{scalar} = \gamma_5,\ \gamma_0\gamma_5,\ \hat{\eta}_{l,\text{conn}} = \mathbb{1},\ \gamma_i\gamma_0,\ \gamma_i,\ \gamma_i\gamma_0\gamma_5,\ \gamma_0,\ \gamma_i\gamma_5\right) \tag{6}$$

- Further operators related to the pseudoscalars η/η':

$$\hat{O}_\eta \equiv \left(\hat{\eta}_{s,\text{conn}},\ \hat{\eta}_{\text{conn}}, \hat{\eta}'_{\text{conn}},\ \hat{\eta}, \hat{\eta}',\ \hat{\eta}_{8,\text{conn}}, \hat{\eta}_{1,\text{conn}},\ \hat{\eta}_{8,\text{disc}}, \hat{\eta}_{1,\text{disc}},\ \hat{\eta}_8, \hat{\eta}_1\right) \tag{7}$$

- Operators evaluated within the Distillation analysis framework:

$$\hat{O}_{\text{Dist}} \equiv \left(\hat{\pi}^+_{\text{full}},\ \hat{K}^+_{\text{full}}\right) \tag{8}$$

- Eventually, there are a few operators dedicated to the topological charge density. Using an improved version of $\hat{q} \propto tr[\tilde{F}_{\mu\nu}F_{\mu\nu}]$ means that q is a gauge field-based variant of the charge. The indices indicate the number of HYP-smearing steps.

$$\hat{O}_{\text{q}} \equiv \left(\hat{q}_5,\ \hat{q}_{10},\ \hat{q}_{30},\ \hat{q}_{50}\right) \tag{9}$$

The set $\hat{O}_{\text{U}}$ consists of "unique" correlators (operators) that are considered to be statistically sufficiently independent from each other. Later, it is used to extract features of $\Gamma[c_{\hat{o}_i}, c_{\hat{o}_j}](t)$, characteristic of the ensemble.

$$\hat{O}_U = \left(\hat{O}_l,\ \hat{\eta}_{s,\text{conn}},\ \hat{O}_{\text{Dist}},\ \hat{\eta}_{8,\text{conn,Dist}}, \hat{\eta}_{1,\text{conn,Dist}}\right) \tag{10}$$

2. Entropy and the effective number of measurements

As depicted in fig. 2, the fluctuation fields possess long and involved AC functions. In particular, there are significant waves resembling harmonic oscillations; the AC does not seem to decay for large $\Delta\tau$. Here, standard statistical analysis methods can not be applied anymore: the method by U. Wolff [2] requires the estimation of the integrated AC time; in general, the variance is expected to be $\sigma^2 = 2\tau_{\text{int}}\Gamma(0)/N$. The Madras-Sokal formula [3] can only be applied to so-called stationary stochastic processes. However, the existence of AC oscillations clearly implicates a dependence

[1]Removing the time-average on a per-configuration basis often leads to improved visibility of AC oscillations or uncovers different features like other modes. The connected pseudoscalar fluctuation fields are dominated by time-like averages $\langle c\rangle(\tau)$. The averages may be related to non-zero topology $Q \neq 0$ - analogously to $Q\neq 0$ contributions to disconnected fields.

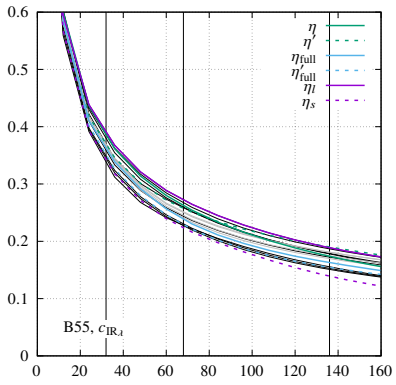

(a) λ-dependence of IR-amplitudes

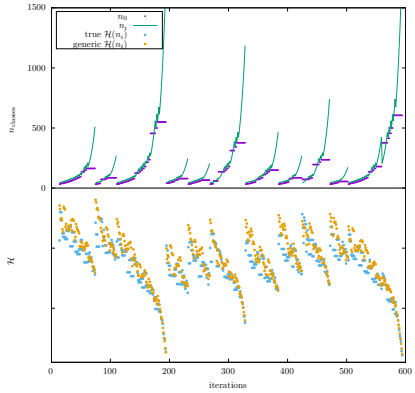

(b) Multiple runs of the algorithm for determining the resolutions of histograms.

Figure 1: τ decay of the amplitudes $(\sigma_{\tau,t}[c_\lambda]/\sigma_{\tau,t}[c_{\lambda=0}])$ **(LHS)** of fields $c_{\hat{o},\lambda}$ as a function of the τ-smoothing scale: this characterizes the fraction of the remaining signal at λ. The set of light-connected correlators $\hat{O}_l$ (6) is depicted by black lines. The correlator corresponding to $\hat{\eta}_l$ (solid purple) is (among) the correlators maintaining high levels of their original signal. η_s (dashed purple) loses significantly more. The η- & η'-connected correlators (green) also hold a relatively high fraction of the signal. The disconnected contributions of full (physical) $\eta(')$ correlators seem to promote signal loss (further emphasized for $\tilde{c}$, not shown). For fields $\tilde{c}$ (5), the reduced signal loss of η_l, η, η' is emphasized (not shown). The scalar connected-correlator is equally resistant (highest black line). Grey lines correspond to topology-amplitudes of $\hat{O}_q$ (9). The AC oscillations shown in fig 2 correspond to amplitudes at the 2nd vertical line ($\lambda = 34$).
Multiple iterations of the algorithm for determining the resolutions of histograms (RHS). As long as there is a significant difference between the entropy of a histogram with n_i classes produced, from data set A with an artificially restricted resolution ($n_0 \leq n_i$ classes), and the entropy of a histograms (also n_i classes) of the true data distribution B, the resolution n_0 must be increased. If the n_0 classes would contain no additional information, n_i could be raised indefinitely without finding a difference.

on the iteration number τ and, thus, renders the process which generated $c_{\hat{o}}$ non-stationary[2]. A possible way out could be to define an effective number of independent DOF (measurements) by relating the amount of information contained in a data set without AC to a corresponding set with AC. This can be achieved by considering the entropy $\mathcal{H}$:

$$N_{\text{eff}}[c] \;\propto\; \mathcal{H}[p[c_a](v;t,\tau)]\;,$$

where p represents the probability distribution of values v from the image of $c_a(t,\tau)$ and t,τ expresses p's dependence on those variables. Both aspects are described sufficiently by autocorrelation & covariance between $c_a(t,\tau)$ and $c_a(t+\Delta t,\tau+\Delta\tau)$ (if $p[c_a] \propto$ (multi) normal distribution.) Let C be this correlation matrix[3]. The Shannon entropy then becomes:

$$\mathcal{H}[c] \;=\; \log\left(\sqrt{2\pi}\,\det(C)\;\right) + \text{length}(C)/2\;, \tag{11}$$

[2]While the HMC algorithm might be non-stationary in a strict sense, for physical observables, AC oscillations are dominated by exponentially decaying AC, and the HMC can, thus, effectively be considered stationary.

[3]C is a block matrix: there are $N \times N$ blocks. Each block describes the t-dependence & has size $T/2 \times T/2$. For this work, it is sufficient just to consider one time-slice, then C reduces to $N \times N$.

which reduces to the well-known Shannon entropy of $m \equiv \text{length}(C)$ normal distributions

$$\mathcal{H}[\mathcal{N}(x,\mu,\sigma)] \;=\; \log\left(\sqrt{2\pi}\sigma\right) + 1/2 \tag{12}$$

if C diagonal. The 2nd part of the definition of N_{eff} consists of normalising (11) with this AC-free version of C. Thanks to the normalisation we do not need to worry about units of information (bits, nats):

$$N_{\text{eff}}[c] \;\equiv N\frac{\mathcal{H}[C]}{\mathcal{H}[\text{diag}_\tau(C)]} \;=\; N\frac{\log\left(\sqrt{(2\pi)^m \det^2(C)}\right) + m/2}{\log\left(\sqrt{(2\pi)^m \det_l^2(\text{diag}_\tau(C))}\right) + m/2} \tag{13}$$

2.1 Entropy of continuous distributions

The naive generalisation of $\mathcal{H}$ from discrete to continuous p distributions is flawed: this can be easily seen by making (12) negative via setting $\sigma^2 < 1/2\pi e$. Jaynes [4] suggested fixing the issues by introducing a reference distribution $r(x)$, which could be understood as resolution of p:

$$\mathcal{H} \;\equiv -\int p(x)\log\frac{p(x)}{r(x)}\,\mathrm{d}x\;,\; r(x) \text{ uniform distribution.} \tag{14}$$

We briefly description of an algorithm that scans for the minimal entropy of $r(x)$ in fig. 1. The term will appear in the numerator & denominator of (13) and increases N_{eff}. It is included in the further analysis but one may argue very well in favour of dropping the term: the effective number of measurements must not depend on the amount of information learned from a single measurement. The computation of $\det(C)$ is challenging. It must be repeated for each $\Delta\tau$ in order to obtain $\Gamma(\Delta\tau)$'s error, but can be accelerated by making use of C being a Toeplitz matrix.

3. Oscillating autocorrelation and space-time modes

Fig. 2 depicts the autocorrelation $\Gamma[c_{\hat{o}}, c_{\hat{o}}](t,\Delta\tau)$(2) for $\hat{o} = \hat{\eta}_{l,\text{conn}}$ as well as for $\hat{o} = \hat{\eta}_{s,\text{conn}}$. Both correlators feature a harmonic AC oscillation, but $c_{\hat{\eta}_l}$ is way more affected. Both oscillations are significant according to the error bands defined by the standard deviation divided by $\sqrt{N_{\text{eff}}}$ (13). The $\hat{\eta}_{l,\text{conn}}$-plot additionally shows the standard statistical error (lighter band): it is ill-defined because of requiring the AC to decay to zero. However, the standard error can be formally computed by assuming the $\Gamma(\Delta\tau) = 0$ for all $\Delta\tau > \min_\tau(\Gamma(\tau) \leq 0)$. Now, if the error is believed to be underestimated because of the truncated AC, one already has implicitly recognized significance of the depicted AC beyond the first extrema. There are plenty of other hints in favour of the oscillations being real. For example, the autocorrelation matrix C virtually consists of the depicted AC oscillations. If (C) is truncated as described before, the determinant of C often turns out to be < 0. This contradicts the fact that correlation matrices are positive-definite by definition. Furthermore, figs. 4 indicate that AC oscillations are space-time dependent: they seem to go along with time-like modes which leads chequerboard-like patterns becoming visible when plotting matrices $\Gamma_{\Delta\tau}(t_1,t_2) \propto \langle c(\tau,t_1)\cdot c(\tau+\Delta\tau,t_2)\rangle_\tau$ for fixed $\Delta\tau > 0$.

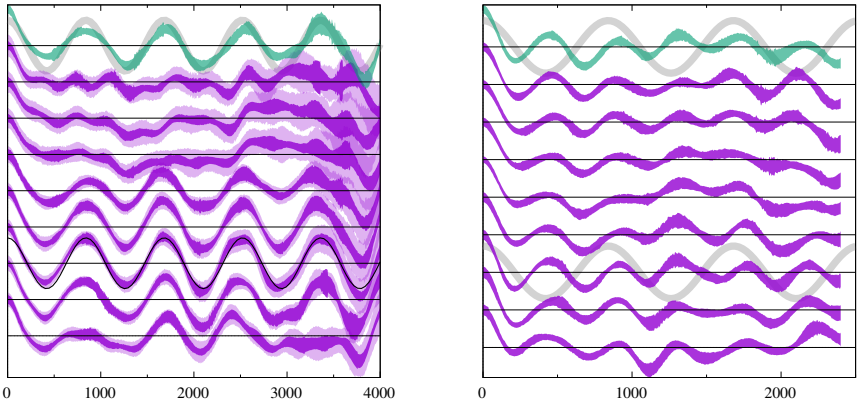

Figure 2: Autocorrelation $\Gamma(\Delta\tau)$ of $\eta_{l,\mathrm{conn}}$ (LHS) for various τ-smoothing scales λ and time-slices (stacked plots): each cell has a height of one, the lowest graph corresponds to $t = 0$ and t increases by four when going one graph up.) The green graphs correspond to the autocorrelations of t-averaged fields. The black line (LHS, t=8) is a cos-function fitted to the $\eta_{l,\mathrm{conn}}$-AC (t=8). It is mirrored by the grey bands to allow for easy frequency comparisons. **RHS:** the same but for $\eta_{s,\mathrm{conn}}$. The frequency of $\eta_{s,\mathrm{conn}}$ appears to be $\approx 5/3 f(\eta_{l,\mathrm{conn}})$, $f(\hat{q}_{10}) \approx 7/3 f(\eta_{l,\mathrm{conn}})$. Most observables $\in \hat{O}_l \cup \hat{O}_\eta \cup \hat{O}_{\mathrm{Dist}} \cup \hat{O}_q$ seem to show oscillations for some λ, but there are no obvious frequency relations between them.

4. A scoring system for oscillations

When we increase λ, more pronounced but lower-frequency modes replace noisy high-frequency modes. It is rather difficult to assess objectively by eye how much the AC function of a correlator is dominated by harmonic oscillations. Furthermore, a simple score would help to compare AC oscillations of different correlators. One of the simplest possibilities is the integrated absolute AC $\bar{\mathcal{I}}_0$: oscillations do not decay for large $\Delta\tau$, so they contribute much to $\mathcal{I}_0$. A more sophisticated version is based on the Fourier transform $\mathcal{F}_\tau[\Gamma[c_\lambda]](f)$, which yields a vector: indices correspond to frequencies and the values of elements are the frequencies' amplitude. Then, the Fourier score can be defined as the ratio of $L_{p=1}$ and $L_{p=2}$ norms:

$$\bar{\mathcal{F}}_0[c_\lambda] \equiv \frac{|| \mathcal{F}[\Gamma[c_\lambda]] ||^2_{p=1}}{|| \mathcal{F}[\Gamma[c_\lambda]] ||^2_{p=2}} \tag{15}$$

The quantity becomes larger if the spectrum of the autocorrelation $\mathcal{F}[\Gamma]$ is dominated by fewer frequency spikes and is low for a densely populated spectrum. Hence,

$$\Gamma[c_o] \text{ oscillates more than } \Gamma[c_{o'}] \;:\Leftrightarrow\; \mathcal{F}_0[c_o] > \mathcal{F}_0[c_{o'}] \,.$$

The dependence on λ can be integrated out using the amplitudes A_λ (fig. 1a):

$$\mathcal{I}_0 \equiv \langle A^2_\lambda \bar{\mathcal{I}}_{0\,\lambda} \rangle_{\lambda\in\Omega_\lambda} \,, \quad \mathcal{F}_0 \equiv \left\langle A^2_\lambda \bar{\mathcal{F}}_{0\,\lambda} \right\rangle_{\lambda\in\Omega_\lambda} \quad \text{with } \Omega_\lambda = \{1;\, 3, 6, 9,\, \ldots, 120\} \tag{16}$$

From fig. 3 follows that the pseudoscalar channel $\eta_{l,\mathrm{conn}}$ and scalar channel are most affected.

In order to cross-check the findings, we generate random datasets that imitate our real ensembles, from those, compute a synthetic $\mathcal{F}_0$ distribution and, eventually, estimate the likelihood of to draw the real $\mathcal{F}_0$-distribution (of the "unique" operators $\hat{O}_U$ (10)) - or a distribution that scores even higher. In slightly more detail, we:

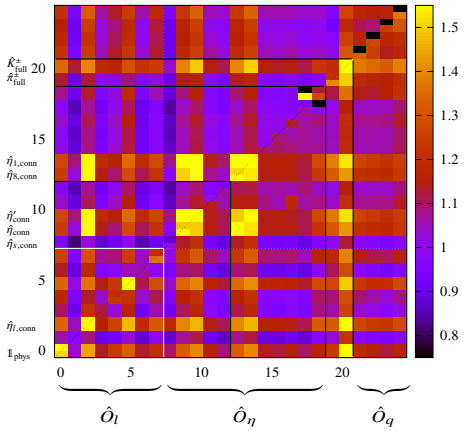

(a) $\mathcal{F}_0$ and $\mathcal{I}_0$ of for various $c_{\hat{o}_i\hat{o}_j}$

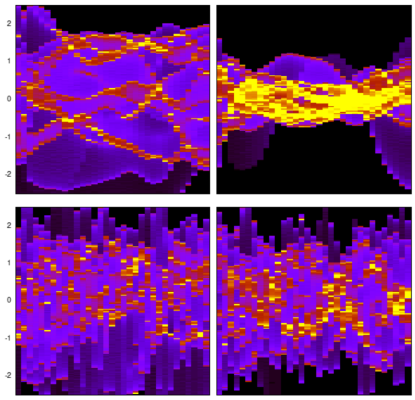

(b) Distributions of $c_{\hat{o}\hat{o}}(t)$ for $\hat{o}$ = scalar (top), $\hat{o} = \gamma_0\gamma_5$(tm) (bottom),

Figure 3: Oscillations scores (LHS): $\mathcal{F}_0$-scores (lower right triangle) and $\mathcal{I}_0$ (upper triangle) for physical 2pt-correlators made from the operators $\hat{O}_U$ (10): $\mathcal{F}_0[o_i(0)o_j(t), o_j(0)o_j(t)]$ defines the $i>j$-element (and the same for $\mathcal{I}_0$ if $i \leq j$) via the i-th operator in $\hat{O}_U$. The plot is divided into sections corresponding to the operator tuples. Of most importance is the inner sector (white line) associated with light, connected correlators from $\hat{O}_l$. The key insight is that scalar and pseudoscalar connected correlators ($\mathbb{1}_{\text{phys}}$, $\hat{\eta}_{l,\text{conn}}$) have the highest scores among the connected correlators. Within the group of η-related operators $\hat{O}_\eta$, (7), the connected correlators stand out: the principal connected correlators (2nd,3rd) and the connected octet/singlet correlators (6th,7th). Note that the disconnect correlators score lower. Operator $\hat{K}^{\pm}$ (evaluated with Distillation) indicates that not only η-related channels are affected (Distillation may promote oscillations: the QCD spectrum is approximated by eigenmodes of the Laplacian, which are waves too.
Distributions of connected $c_{\hat{o}\hat{o}}$ (RHS): with $\hat{o} = \mathbb{1}_{\text{Phys}}$ (scalar, top) and $\hat{o} = \gamma_0\gamma_5$ (twisted basis, bottom), λ=132. The smoothing (3) deforms the Gaussian distr. of the scalar c (pseudoscalar looks similar) into a discrete spectrum. From a pure harm. AC oscillation one would expect accumulation at c's extrema. The accumulations form continuous functions over $t \in [0, T/2]$ (x-axis), some being waves other being more const. Those might be the reason why (5) collapses the spectrum of the $\tilde{c}$ (very RHS). The distr. of typical connected c,$\tilde{c}$ (represented by $\hat{o} = i\gamma_0\tau_3$) remain Gaussian-like for $\lambda > 0$ and $\tilde{c}$.

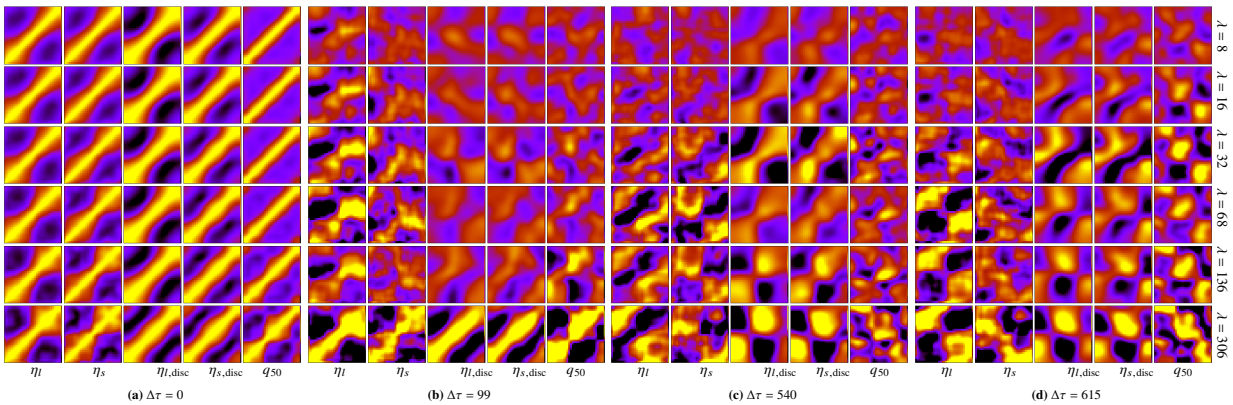

(a) $\Delta\tau = 0$ **(b)** $\Delta\tau = 99$ **(c)** $\Delta\tau = 540$ **(d)** $\Delta\tau = 615$

Figure 4: Time-like correlation $\Gamma_{\Delta\tau}(t_1, t_2)$ for various $\Delta\tau$. The colour range is (black-yellow $\leftrightarrow [-0.2, +0.2]$) for all $\Delta\tau = 0$ and fixed to $\leftrightarrow [-0.4, +0.4]$ for $\Delta\tau > 0$. $\Gamma_{\Delta\tau}$ returns to high levels of autocorrelation on a regular basis. Those peaks often occur in combination with an (anti-) diagonal pattern and the chequerboard pattern. The AC-oscillation is faster for smaller λ. The $\Delta\tau = 0$ case shows that t=0 and t=$T/2$ are strangely correlated. (In [5] such an observation was attributed to low statistics, which it does not seem to be.)

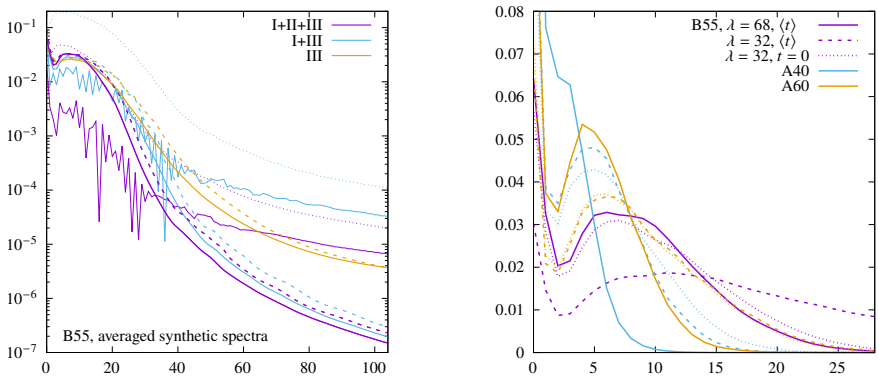

Figure 5: Sample averages of the synthetic AC spectrum (LHS) and of the lattice AC spectra (RHS) : Synthetic spectra imitating B55 ($\lambda = 68$) are shown on the LHS for various combinations of the steps 4 for reducing finite-data artefacts. Steps I+II+III result in the narrow spectrum (bold magenta), which is used for fScore computation. The spectrum broadens moderately without cut-off averaging (I+III, bold blue). When the signal ends abruptly (no I), a wide range of artificial frequencies emerges (orange). For $f < 20$, the standard deviations (dotted lines) are of the same order as the spectra themself. Without smoothing individual samples (step III), even the average remains noisy (thin graphs).
The synthetic spectra of B55, A60 & A40 are compared on the RHS. The existence of the peaks ($3 \lesssim f \lesssim 13$) means that our AC-analysis of fluctuations tends to produce wave-like contributions randomly. Those contributions turn out to be insufficient to explain the AC oscillations from real data. Decreasing the amount of IR-smoothing λ=68 $\rightarrow$ λ=32 broadens the spectra of B55, A40 & A60 consistently. B55's deviating behaviour of the t=0 time slice hints at a noisy extraction of typical fluctuation lengths.

1. Choose a IR-smoothing length λ.
2. For the set made of interpolating fields $\hat{O}_U$: fit the exponential model $A\exp[-\tau^2/(\epsilon^2+\lambda^2)] + B\exp[-(\tau-\mu)^2/(\bar{\epsilon}^2+\lambda^2)]$ to the ACs (the last term helps to fit the 1st minimum, which supposedly belongs to the AC oscillation, and prevents the underestimation of ϵ, thereby.) $\rightarrow$ A set of 13 values $\{\epsilon_o\}$ characterizing the lengths of the assumed Gaussian AC fluctuations.
3. For each ϵ_o, create synthetic samples: Gaussian bells with $\sigma = \epsilon_o$ placed at random positions τ with discrete random amplitudes (because of fig. 3b).
4. We perform the AC analysis on the samples of the synthetic data set.
5. Fourier transform the results to obtain the synthetic frequency distribution $p[\mathcal{F}_6]$.
6. From Fourier transforms of the $T/2$ ACs of the 13 operators $\in \hat{O}_U$ we obtain the few (416) frequency graphs containing presumably real oscillations.
7. Compute the likelihood of drawing 416 samples from the synthetic $\mathcal{F}_6$-distribution that score equal or higher.

For B55, A40 & A60, those likelihoods turn out to be almost zero. Plot 6 shows that the real data's $\mathcal{F}_6$-values overlap with the synthetic distribution widely, but a couple of higher scores lead to the vanishing probability. Because of the finite length of our data sets, naive Fourier transforms are plagued by artefacts. The following steps resulted in a noticeable improvement (see fig. 5).

I. In order to make the signal ends fade out, they are folded with half of a Gaussian bell over the length of $l \equiv 2\sigma \approx \frac{1}{3} \cdot$ data set length N. This step provides most of the artefact reduction.
II. The previous step tends to introduce high-frequency modes into the frequency space itself. Averaging the spectra corresponding to multiple values of length $l \in [\frac{1}{2}, \frac{1}{3}] \cdot$ signal length N

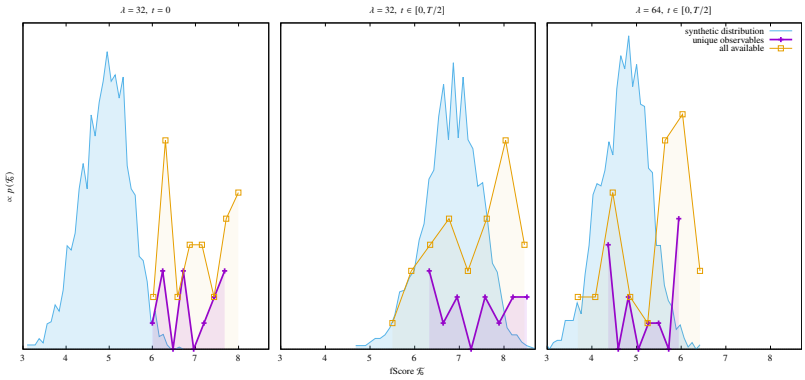

Figure 6: Synthetic fScore distributions (blue) compared to fScores of lattice data (magenta, orange): the distribution of fScores for a collection of correlators that are considered sufficiently unique O_U (magenta) and the distribution of an extended set, containing many $\eta(')$-related correlators (orange), are compared with the fScore-distribution of synthetic data. The synthetic data was modelled to contain fluctuation of the same length as their lattice equivalent but scores lower: Hence, the likelihood of the real lattice data's harmonic AC oscillations being a random artefact turns out to be tiny. (The lattice data graphs have been rescaled for better visibility. There are not enough unique correlators for computing their histograms reliably.) Using time slice $t = 0$ only (left) and increased IR-filtering (right) seem to promote AC oscillations.

reduces the issue thanks to destructive interference.

III. Remaining high frequencies are filtered out by smoothing the resulting spectra with a Gaussian bell with $\sigma = N/512$.

5. Conclusions

There is plenty of evidence in favour of AC oscillations. The Fourier score $\mathcal{F}_0$ and $\mathcal{I}_0$ suggest that pseudoscalar and scalar connected meson correlators contain the most articulated AC oscillations, which can also be confirmed by visual inspection of the AC. Nevertheless, oscillations can be found for most of the investigated channels (for oscillating topology see the talk slides & an upcoming paper.) This suggests that it is not a single physical phenomenon that is responsible but the HMC algorithm itself. The canonical momenta used by the Molecular Dynamics (MD) step to propose updated fields for $\tau + 1$ enhance the 4D QCD dynamics in the τ-dimension. In conjunction with a potential term, contributed by the QCD Lagrangian, harmonic oscillations become possible. Indeed, the Fourier Acceleration (FA) [6] approach assumes that the evolution speed of fields can be assessed by assuming modes (with respect to τ): the idea is to determine associated mass terms from the Lagrangian and to equalize those by manipulating the kinetic MD term. Consequently, modes oscillate with similar frequencies and critical slowing-down is suppressed. Recently, a FA project has shown that oscillations are produced by their simulation algorithm [7], but it was assumed that those waves are connected to free fermionic modes and that Landau gauge fixing is a prerequisite. Lüscher's analysis [8] deals with the 5D Φ^4 theory of the HMC. Most notably, the corresponding EOM (17) can be solved via a kernel function (18):

$$\partial_\tau^2 \phi(x,\tau) \;=\; -\frac{\delta}{\delta(x,\tau)} S[\phi(x,\tau)] - 2\mu_0 \delta_\tau \phi(x,\tau) + \eta(x,\tau)\,, \tag{17}$$

$$K_{\mathrm{GHMC}}(x,\tau) \;=\; \theta(\tau) \int \mathrm{d}^4 q\, \frac{e^{iqx}}{(2\pi)^4} e^{-\mu_0 \tau} \frac{\sin(\epsilon_q \tau)}{\epsilon_q}\,,\; \epsilon_q = \sqrt{q^2 + m_0^2 + \mu_0^2}\,. \tag{18}$$

Here, we already have τ-oscillations, though they are suppressed exponentially. I believe this approach is a promising ansatz towards understanding of observed AC oscillations. It is noteworthy that the scalar and pseudoscalar channels with the largest oscillation contributions, can be described by Klein-Gordon fields and thus Φ^4 theory. Christ and Wickenden [9] have extended the work [8]: they show that in a Fourier accelerated Φ^4 theory, the above AC modes (18) decouple from their space-time contributions. Hence, when FA could be made to remove the observed coupling from LatticeQCD (fig. 4a), we would gain strong evidence that the AC oscillations are explained by (18). In closing, I would like to give three ideas on how motions in τ could survive the randomization of MD momenta at the beginning of each trajectory. In theory, this step and the Metropolis test should maintain ergodicity, however:

1. The 2nd law of thermodynamics also holds for the MC time τ. For example, pair-created excitations with few updates spatially separated are not likely to wander on top of each other again.
2. If the motion is linked to spatially extended excitations, local momentum randomization may cancel globally.
3. The 5D MD forces might bring the system into a state of high potential energy at the end of each trajectory, which in turn restarts the MD motions at the beginning of the next trajectory.

References

[1] K. Jansen, C. Urbach, *tmLQCD: A Program suite to simulate Wilson Twisted mass Lattice QCD*, *Comput.Phys.Commun.* **180** (2009) 2717 [0905.3331].

[2] ALPHA collaboration, *Monte Carlo errors with less errors*, *Comput. Phys. Commun.* **156** (2004) 143 [hep-lat/0306017].

[3] M. Luscher, *Schwarz-preconditioned HMC algorithm for two-flavour lattice QCD*, *Comput. Phys. Commun.* **165** (2005) 199 [hep-lat/0409106].

[4] E.T. Jaynes, *Information theory and statistical mechanics*, *Brandeis University Summer Institute: In K. Ford (ed.). Statistical Physics (PDF). Benjamin, New York* **3** (1963) 181.

[5] C. Alexandrou et al., *Phys. Rev. D* **101** (2020) 034519 [1908.10706].

[6] G.G. Batrouni, G.R. Katz, A.S. Kronfeld, G.P. Lepage, B. Svetitsky, K.G. Wilson, *Langevin Simulations of Lattice Field Theories*, *Phys. Rev. D* **32** (1985) 2736; b) S. Duane, R. Kenway, B.J. Pendleton, D. Roweth, *Physics Letters B* **176** (1986) 143; c) S. Duane, Pendleton, *Phys. Lett. B* **206** (1988) 101; d) Davies, Batrouni, Katz, Kronfeld, Lepage, Wilson et al., *Phys. Rev. D* **37** (1988) 1581.

[7] A. Sheta, Y. Zhao, N.H. Christ, *Gauge-Fixed Fourier Acceleration*, *PoS* **LATTICE2021** (2022) 084 [2108.05486]; b) Y. Zhao, *PoS* **LATTICE2018** (2018) 026 [1812.05790].

[8] M. Luscher, S. Schaefer, *Non-renormalizability of the HMC algorithm*, *JHEP* **04** (2011) 104 [1103.1810].

[9] N.H. Christ, E.W. Wickenden, *Fourier acceleration, the HMC algorithm and renormalizability*, *PoS* **LATTICE2018** (2018) 025 [1812.05281].